

Microelectrode Study of the Genesis of the Monophasic Action Potential by Contact Electrode Technique

BJÖRN C. KNOLLMANN, M.D., PH.D.,* JOSEPH TRANQUILLO,‡
 SYEVDA G. SIRENKO, PH.D.,* CRAIG HENRIQUEZ, PH.D.,‡
 and MICHAEL R. FRANZ, M.D., PH.D.*†

From *Georgetown University and †VA Medical Centers, Washington, DC; and ‡Duke University, Durham, North Carolina

Monophasic Action Potential Genesis. Introduction: Despite widespread use of the contact electrode for recording monophasic action potentials (MAPs) in both clinical and experimental research, the mechanism underlying the genesis of the contact MAP remains unproven. The “Franz hypothesis” assumes that the MAP is driven by a current source originating at the boundary between cells depolarized by the MAP electrode pressure and normal cells immediately adjacent to it. To date, no direct experimental data exist to support this hypothesis.

Methods and Results: In 10 Langendorff-perfused mouse hearts, a miniaturized MAP probe was inserted into the right ventricle (RV) and gently pressed against the endocardium of the upward-facing RV free wall. During stable contact and stable MAP recording, KCl-filled glass microelectrodes were lowered from above the RV to record transmembrane action potentials (TAPs) at the center of and 0.05 and 0.2 mm outside the perimeter of the MAP electrode contact site. TAPs at the center had normal resting potentials (RP) in epicardial layers (-78 ± 4 mV) but showed gradual decrease toward deeper layers, reaching a minimum RP of -23 ± 0.8 mV directly above the MAP electrode surface. RPs at 0.05 mm outside the MAP perimeter were normal at the epicardial surface and with increasing transmural depth showed significantly less decrease than central recordings (min RP -41 ± 0.8 mV, $n = 11$, $P < 0.00001$). TAPs at 0.2 mm from the MAP electrode perimeter had normal RPs across the entire RV wall.

Conclusion: These direct data are the first to support the hypothesis that the MAP is generated locally through pressure depolarization of a circumscribed volume of cells that (1) has sharp voltage gradients toward normal cells, (2) provides a strong local current source, and (3) when simulated with a circuit model creates the field potential recorded by the contact MAP electrode. (*J Cardiovasc Electrophysiol*, Vol. 13, pp. 1246-1252, December 2002)

monophasic action potential, genesis, modeling, microelectrode, isolated heart

Introduction

The contact electrode technique was introduced in 1983¹ as a gentler and safer method to record monophasic action potentials (MAPs) compared to suction electrodes² and other techniques using frank tissue injury.³ This technique was validated by showing that contact MAPs and transmembrane action potentials (TAPs) recorded simultaneously at directly adjacent sites had virtually congruent voltage time courses.⁴⁻⁶ Due to its safety and simplicity, as well as high stability and recording fidelity, the contact electrode technique has been widely used in clinical and experimental research (994 publications listed in MEDLINE to date), including pharmacologic interventions, myocardial ischemia, arrhythmia ablation, cardiac memory, and other repolarization-related phenomena in both ventricular and atrial myocardium (reviewed by Franz⁷). Despite this widespread use of the contact MAP, the mechanism under-

lying the genesis of the MAP by contact electrode remains unexplained. How can an electrode many times too large to enter a single cell so accurately depict the voltage time course of cellular action potentials in its immediate vicinity?

Because early methods of MAP recording used direct myocardial injury (cutting, stabbing, or suctioning a small area of the myocardium), MAPs were interpreted as “injury potentials.” As such, in 1932 Schuetz⁸ assumed that the MAP represented the voltage drop between the potential of injured cells and neighboring intact cells. This “injury potential” theory assumed an unspecified gradient between cells that were depolarized by injury and adjacent or distant cells that underwent normal cellular depolarization and repolarization. This theory further assumed a discrete potential difference to be responsible for the MAP genesis; in other words, the MAP was thought to be caused by a *voltage* source. Franz, after showing that contact electrode MAP recordings were not reduced by shunting of the extracellular resistor, hypothesized that the contact electrode MAP is caused by a *current* source.^{1,7,9} This hypothesis has been supported by other investigators¹⁰ and assumes that a circumscribed volume of cells directly underneath the contact electrode is depolarized and rendered nonexcitable by mechanical pressure, whereas cells outside the contact area retain normal membrane potentials, excitability, and electrical coupling with the depolarized tissue.

To date, this hypothesis has remained unproven. There

This study was supported by American Heart Association Scientist Development Grant 0130285N and Pharmaceutical Research and Manufacturers of America Foundation Faculty Development Award to Dr. Knollmann.

Address for correspondence: Michael R. Franz, M.D., Ph.D., Cardiology Division, VA Medical Center, 50 Irving Street NW, Washington, DC 20422. Fax: 202-745-8473; E-mail: mfranz@washington.va.gov

Manuscript received 18 June 2002; Accepted for publication 3 October 2002.

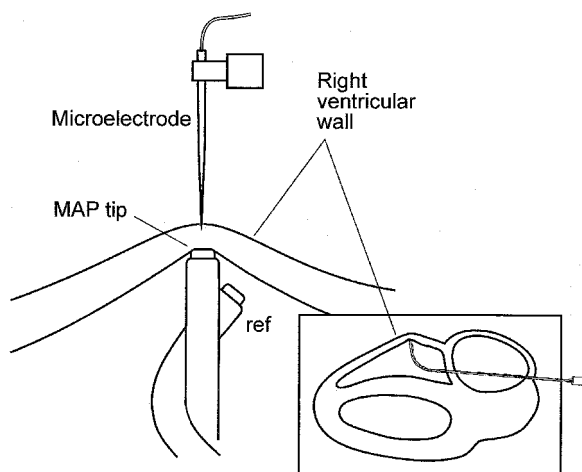


Figure 1. Experimental setup of isolated perfused mouse heart.

are no direct experimental data showing that cells underneath the MAP contact electrode are depolarized and, if they are, to what extent and how sharp the border between depolarized and normal cells is. The aim of this study was to probe with conventional glass microelectrodes the distribution of TAPs in the tissue directly surrounding the MAP electrode tip. Earlier problems of recording TAPs directly underneath the MAP electrode were overcome by using a thin-walled mouse right ventricle (RV) with the MAP and TAP electrode juxtaposed on either side. This allowed us to measure TAPs in the immediate vicinity and directly underneath the MAP contact electrode.

Methods

Experiments were performed in 10 isolated Langendorff-perfused mouse hearts. This preparation was chosen because the small heart size with its thin ventricular walls made it easier to interrogate the ventricular wall transmurally by glass microelectrodes. We recently developed a miniaturized MAP electrode for the mouse heart and validated its accuracy against TAP recordings,⁵ providing an important prerequisite for this study. Experiments were performed in strict adherence to the National Institutes of Health (NIH) guidelines on research in experimental animals and were approved by the Georgetown University animal care and use committee.

Experimental Setup and Procedures

Hearts were excised and prepared for Langendorff perfusion as described previously.⁵ In brief, this setup resulted in a horizontally cradled heart with the RV facing upward. The custom-built miniature Ag-AgCl MAP contact electrode probe⁵ was inserted through a cut in the right atrium and then through the tricuspid valve into the RV (Fig. 1). The 90° deflected MAP electrode tip was pointed upward and made to impinge against the endocardium of the RV free wall. This spot of contact was noticeable by a “tent pole” appearance of the RV wall and visualized by a darker shadow of the MAP electrode against the relatively translucent surrounding tissue. 2,3-Butanedione monoxime (BDM) 15 mM was added to the perfusate to minimize contractions and thus microelectrode dislodgments. BDM

alters the wave shape of the TAP but does not influence the correlation between MAP and TAP recordings.⁵ Once a stable position that provided quality MAP recordings was found, a standard glass microelectrode was lowered by a micromanipulator onto the epicardium at or around the MAP contact site. A micrometer scale within the binocular microscope was used to gauge the distance of the microelectrode tip from the center of the MAP electrode contact site. TAPs were recorded using KCl-filled (3 M) glass microelectrodes (tip resistance 15–20 MΩ) as previously described.⁵ The custom-built input stage of this microelectrode recording setup consisted of a high-impedance solid-state operational amplifier coupled as voltage follower with capacitance compensation (“driven shield”). The heart was connected to system ground via an Ag-AgCl bath electrode.

Measurement of Intracellular Membrane Potential in the Vicinity of the MAP Electrode

The tissue distribution of transmembrane resting potentials (V_m) surrounding the MAP electrode tip was measured in two dimensions (transmural and apicobasal) as follows. First, the microelectrode was lowered perpendicularly onto the epicardium at a distance of approximately 0.2 mm from the perimeter of the MAP tip in an apicobasal axis (the MAP electrode tip was easily recognized as a dark shadow transmitted through the thin RV free wall). After the first successful impalement, the TAP was advanced in 10- μ m steps with the micromanipulator into deeper layers, resulting in subsequent TAPs at increasing depths. Due to flexibility of the thin microelectrode shaft and compliance of cardiac tissue, not every step advanced the tip of the electrode. Usually 3 to 5 steps were needed to produce the next successful impalement. This procedure resulted in 6 to 12 successful intracellular impalements for approximately 30 steps before the microelectrode tip entered the RV cavity (recognizable by a potential jump to zero). Rather than attempting to measure the exact location of the microelectrode tip in reference to the epicardial surface, we defined the first successful impalement as subepicardial, the last successful impalement as subendocardial, and distributed all recordings in between along an arbitrary scale of eight layers. Because the RV free wall is about 0.45 mm thick,¹¹ each layer has an approximate thickness of 0.05 mm. Next, we lowered the microelectrode at 0.05 mm lateral distance from the MAP tip perimeter and measured the transmural V_m in similar fashion. Finally, the electrode was moved directly over the MAP electrode for the center recordings. Here a subendocardial TAP (directly adjacent to the MAP electrode surface) was defined as the last TAP recorded before the microelectrode tip touched the MAP electrode surface, which produced an easily recognizable sudden large offset potential. To ensure that a depolarized V_m was not caused by a broken microelectrode, we only analyzed TAP recordings that were recorded with an intact microelectrode. This was tested by using the same microelectrode immediately afterward in myocardial sites distant to the MAP electrode and confirming that TAPs with a normal V_m of at least -70 mV could be obtained.

Statistical Analysis

Data are expressed as mean \pm SE, unless otherwise indicated. Mean values were compared with single-factor

analysis of variance (ANOVA). Reported P values were obtained by post hoc Student's *t*-test analysis performed whenever significant differences were detected by ANOVA.

Results

MAP Recordings

The miniaturized contact electrode produced stable MAP recordings from the RV free wall. RV endocardial MAP recordings exhibited the typical features of murine ventricular action potentials reported in our earlier study⁵: rapid upstroke, steep phase 1 to approximately half the total MAP amplitude, and subsequent gradual repolarization phase until the diastolic potential was reached (Fig. 2, right bottom panel).

TAP Recordings

Microelectrodes were used to explore cellular potentials transmurally across the RV myocardial wall as illustrated in Figure 1. TAPs could be recorded at different depths and distances from the MAP electrode contact site. Figure 2 illustrates how resting potential and action potential amplitude changed as the microelectrode was advanced into

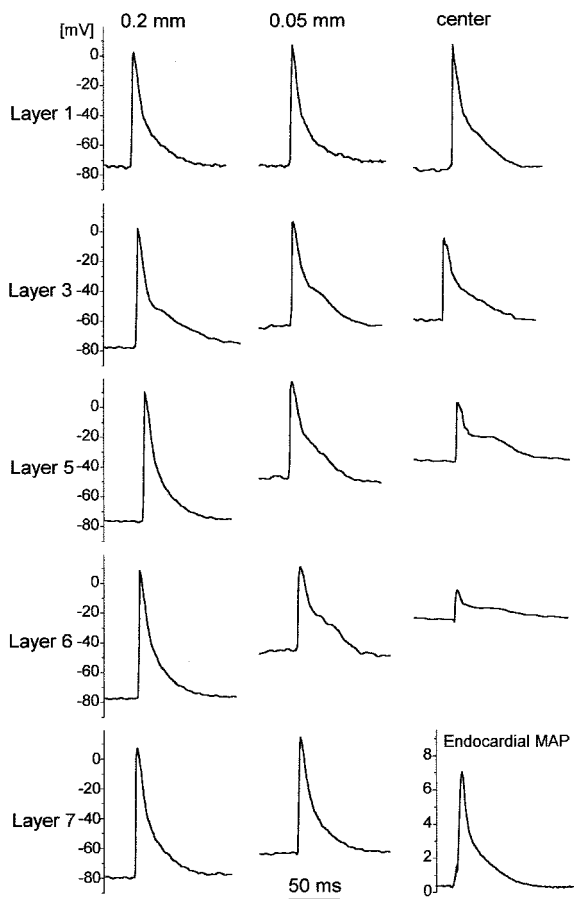


Figure 2. Representative transmembrane action potentials recorded transmurally across the right ventricular (RV) free wall from subepicardial tissue (layer 1) to subendocardial tissue (layers 6 and 7) at sites outside the perimeter of the monophasic action potential (MAP) electrode (0.2 mm, 0.05 mm) and over the center of the MAP electrode surface (center). The MAP electrode remained positioned on the RV endocardial surface, and MAPs were recorded continuously (right bottom panel).

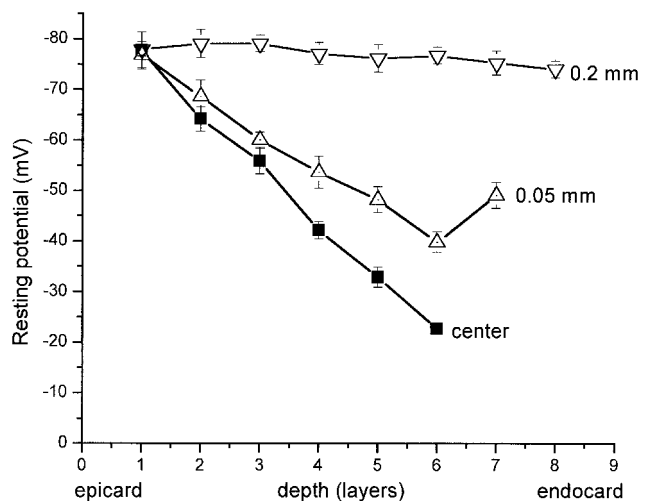


Figure 3. Average resting potentials recorded transmurally across the right ventricular free wall in different depths at sites over the center of the monophasic action potential (MAP) electrode surface (center) and outside the perimeter of the MAP electrode (0.05 mm, 0.2 mm). Layer 1 represents subepicardial tissue; layers 6–8 represent subendocardial tissue.

deeper tissue layers at different recording sites relative to the MAP electrode contact site. Penetration depths were defined as consecutive tissue layers (compare with Methods section and Fig. 4) from subepicardial (layer 1) to subendocardial tissue (layers 6–8, depending on recording site).

TAP recordings at sites 0.2 mm outside the MAP perimeter

TAP recordings at sites 0.2 mm or more outside the MAP perimeter had full action potentials and normal resting potentials across the entire RV wall (Fig. 2, left column, and Fig. 3), with a minimum resting potential of -76 ± 0.8 mV ($n = 10$ sites from 10 hearts, $P < 0.001$ vs both central and 0.05 mm). Successful microelectrode impalements (62 in total) were achieved from 4 to 12 consecutive tissue layers per recording site (mean 6.2 ± 1.0) before the microelectrode tip reached the RV cavity.

TAP recordings at sites 0.05 mm outside the MAP perimeter

Resting potentials at sites 0.05 mm outside the MAP perimeter were normal at the epicardial surface but decreased to a minimum resting potential of -41 ± 0.8 mV ($n = 11$ sites from 10 hearts; Fig. 2, middle column, and Fig. 3). Successful impalements (49 in total) were obtained from 3 to 7 different tissue layers per recording site (mean 4.5 ± 0.3) before the microelectrode tip reached the RV cavity.

TAP recordings at sites over the center of the MAP electrode

TAPs recorded in subepicardial tissue layers directly over the center of the MAP electrode had normal resting potentials (-78 ± 4 mV). Figure 2 (right column) illustrates how resting potential and action potential amplitude declined as the microelectrode was advanced into deeper layers. The resting potential reached a minimum of $-23 \pm$

0.8 mV ($n = 27$ sites from 10 hearts) directly above the MAP electrode surface. This was significantly less compared with peripheral recordings ($P < 0.0001$; Fig. 3). Note that in a total of 103 successful impalements a miniature action potential (amplitude between 10 and 20 mV) always remained in TAPs recorded from tissue layers directly above the MAP electrode. Transient jumps to more “normal” (i.e., -70 mV) resting potentials were never observed. However, only 3 to 6 different tissue layers (mean 3.8 ± 0.3) were discernible before the microelectrode tip reached the MAP electrode surface. These were significantly fewer tissue layers compared with TAP recordings from sites 0.05 and 0.2 mm outside the MAP electrode perimeter ($P < 0.01$ and $P < 0.0001$ vs 0.05 and 0.2 mm, respectively), suggesting that the MAP electrode significantly compressed the overlying heart tissue.

Cell membranes depolarized gradually from normal (-78 mV) to -23 mV in the central position above the MAP electrode (Fig. 3). No “sudden” voltage border was found as the TAP electrode probed downward, with an average voltage drop of 14 ± 1.3 mV per tissue layer (range 4–45 mV). Because the mouse RV is approximately 0.45 mm thick,¹¹ the transmural voltage gradient above the MAP electrode was approximately 122 mV/mm. In contrast, the voltage drop at the border of the MAP electrode in the lateral direction was at least twice as steep. At a distance of 0.2 mm, the membrane potential was already normalized, resulting in lateral voltage gradient of at least 275 mV/mm. Based upon the data collected with the exploring microelectrodes at three different lateral positions, Figure 4 depicts the predicted membrane potential field generated by the MAP electrode. Figure 4 also illustrates both the steeper lateral voltage gradient and the tissue compression over the MAP electrode.

Model of MAP Genesis

The close bipolar MAP electrode¹ records the potential difference between the tip electrode at the surface of the tissue (Fig. 4) and a reference electrode 2 mm away immersed in the tissue bath. The extracellular potential at the

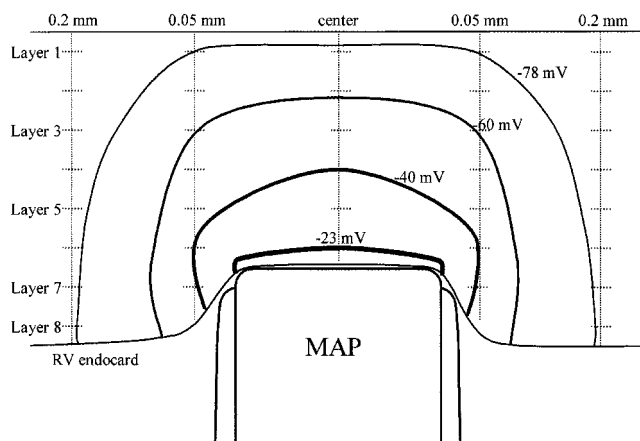


Figure 4. Hypothetical membrane potential field induced by the monophasic action potential (MAP) electrode in mouse right ventricle (RV). Diagram is based on experimental results of Figure 3. Distance between each layer is 0.05 mm; thickness of mouse RV is 0.45 mm; width of MAP tip is 0.25 mm.

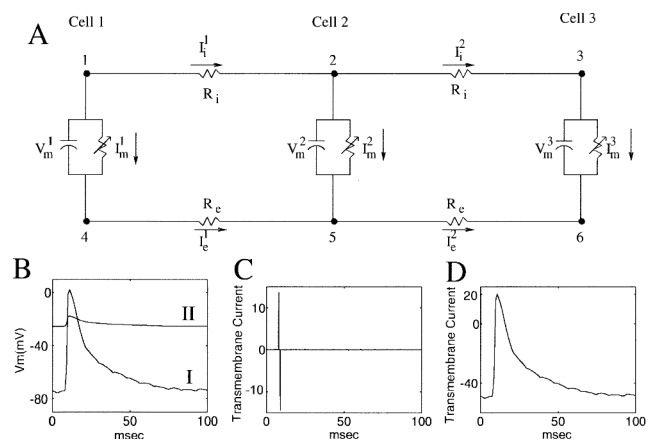


Figure 5. (A) The three-cell circuit model used to determine the transmembrane current sources arising from the coupling of cells with normal and partially depolarized action potentials. (B) Modeled normal (I) and depolarized (II) action potentials. (C) Transmembrane current source at cell 2 arising from the propagation of the action potential in B-I. The magnitude and units of the current are dependent on the scale factor $1/(R_i + R_c)$. (D) Transmembrane current source at cell 2 arising from an action potential propagating into a depolarized region. See Appendix for details.

tissue surface depends on the electrical field generated by the membrane currents in the underlying cells.¹² Because field strength drops with distance from the surface and because the tissue bath is grounded, the contribution of the reference electrode is expected to be very small, and the MAP signal is largely generated by the electrical field potential at the tip electrode.

To explain the origin and shape of the time-varying transmembrane current responsible for the electrical field near the MAP tip electrode, a circuit model was developed. Based on the observation that about one cell length (0.125 mm) lateral to the MAP tip membrane potentials was almost normalized (Fig. 4), we used a simplified three-cell model (Fig. 5A). Using Kirchoff's current laws, it can be shown that the time-varying transmembrane current $I_m(t)$ at the second node is determined by the intracellular and extracellular conductances and the membrane potentials of the adjacent cells (Appendix, Equation 12). A representative mouse transmembrane action potential (Fig. 5B) was used to compute the $I_m(t)$ of cell 2 as described in the Appendix.

If all cells have normal action potentials (shown in Fig. 5B-I), then $I_m(t)$ recorded at the surface of cell 2 has the biphasic time course shown in Figure 5C, reminiscent of a local electrogram. Although the time course and shape of $I_m(t)$ are not exactly the same as the extracellular potential, the work of Plonsey and Fleming¹³ shows that $I_m(t)$ is a good approximation near the surface of the tissue. To simulate an MAP electrode placed onto cell 2, a nonspecific linear leakage current was added in cell 2 (see Appendix). The resulting transmembrane potential under the MAP electrode was attenuated to -23 mV (Fig. 5B-II), as observed experimentally (Figs. 2 and 3). As shown in Figure 5D, $I_m(t)$ is no longer biphasic but has a monophasic time course similar to the transmembrane action potential. Because the scale factor $1/(R_i + R_c)$ is always positive, changes in intracellular/extracellular conductance are predicted to affect only $I_m(t)$ amplitude and thus MAP signal amplitude, not its wave shape. Thus, the genesis of the MAP may be

explained by the close proximity of depolarized and normal myocytes generating a strong electrical field surrounding the MAP tip electrode.

Discussion

This study is the first to report intracellular action potentials (TAPs) in the immediate vicinity of, and within the tissue directly overlaying, the MAP contact electrode site recorded simultaneously with the MAP (Fig. 2). Cells in layers directly overlaying the MAP contact electrode were depolarized to resting V_m diminished by up to -23 mV. V_m gradually increased with distance from the MAP electrode, reaching normal V_m at the epicardial surface directly over the center of the electrode tip (Fig. 3). TAPs recorded from cells as close as 0.05 to 0.2 mm from the contact electrode perimeter maintained normal V_m and TAP amplitudes. This indicates a very sharp border between tissue depolarized by contact electrode pressure and cells in the immediate vicinity of the electrode contact site (Fig. 4). Our modeling studies suggest that this gradient gives rise to transmembrane current sources at the border with a time course that follows the transmembrane potential when a wavefront passes by the electrode (Fig. 5 and Appendix). Direct measurement of the region of depolarization and the nature of the sharp gradient support the current source hypothesis of the genesis of the contact MAP.

Previous Work Related to the Present Study

An early validation study measured TAPs in the immediate vicinity of the MAP electrode in an isolated perfused rabbit septum preparation and found normal TAP resting and action potentials as close as 0.2 mm from the MAP electrode perimeter.⁴ This finding is consistent with that found in the present study. Ino et al.⁶ recorded TAPs in an isolated slice of canine endomyocardium and also found good congruence between the MAP and TAP waveform. In both studies, no TAP recordings could be made directly underneath the MAP electrode because the explored tissue laid flat on a dish and access for microelectrodes to cells underneath the MAP electrode was obstructed by the MAP electrode itself. The present study overcame the methodologic problem of measuring intracellular potentials *directly* underneath the MAP electrode by impaling the myocardial wall from the *epicardial* surface overlaying the MAP electrode and by choosing the mouse heart whose thin RV wall permitted transmural penetration by a glass microelectrode.

Theories on the Genesis of the MAP

The first MAPs were recorded via frank injury to the myocardium, using stabbing, burning, or suction electrodes (reviewed by Franz⁷). As such, the MAP voltage was initially explained by Schuetz⁸ as the difference between the membrane potential of the injured cells and that of normal cells, multiplied by the sum of extracellular and intracellular resistance divided by the intracellular resistance ($V_{inj} = V_m \times [R_e + R_i]/R_i$). According to the Schuetz equation, MAP amplitude is a fraction of the normal TAP voltage and may reach 50% of the TAP voltage when the extracellular resistance equals the intracellular resistance. This assumes that the MAP is driven by a voltage source: the TAP of normal cells reduced by extracellular shunting through elec-

trolytic fluid between the two extracellular electrodes that record the MAP.

The Schuetz "injury potential" theory cannot properly explain the more stable MAP signal produced by contact electrode. Injury potentials are short lived because of rapid "healing over" and electrical uncoupling of the injured tissue, leading to cessation of injury currents.¹⁴ Further, injury potentials usually are a small fraction of an uninjured cell's normal potential and an injured cell's depolarized potential, due to shunting in extracellular space.¹⁵ Franz⁹ reported that the amplitude of the contact electrode MAP is not subject to extracellular shunting; virtually identical MAP amplitudes were recorded by contact electrode regardless of whether the myocardial surface was relatively dry or immersed in fluid or blood.

To account for these experimental results, Franz hypothesized that the contact electrode MAP is caused by the *current* sources near the region of contact.^{1,7,9} This hypothesis has been supported by other investigators.¹⁰ Based on the assumption of cellular depolarization by contact pressure in a nondestructive fashion, core conductor theory predicts that transmembrane *current* sources are produced at the boundary of normal tissue and depolarized tissue, where there is change in potential gradient. The experimental data of this study confirm the postulated presence of a highly localized voltage gradient in the immediate vicinity of the MAP electrode (Figs. 3 and 4). Assuming a uniform volume conductor, the potential field generated by these sources will be greatest near the current source (the boundary of the dominant voltage gradient) and would fall as the inverse of the distance from the source.¹³ Given the sharp boundary between depolarized cells (those underneath the MAP electrode) and normally polarized cells (just outside the MAP perimeter) in close proximity of the recording electrode surface, the resulting field currents should be picked up with relatively little loss by the MAP electrode. Here we present a simple three-cell model to explain the time course of the transmembrane current sources for propagation in normal tissue and propagation near a site with a pressure-induced depolarization. Figure 5C shows the classic finding based on core conductor theory. Under conditions where the front propagates with uniform velocity, such that the wavefront is neither attenuated nor distorted (just time shifted), the time course of the transmembrane current source is biphasic when the upstroke passes and near zero during recovery because of the small potential gradient. In contrast, when normal tissue is adjacent to a region that is depolarized such that the time course of the transmembrane potential is time shifted but not the same at every site, the transmembrane current sources are monophasic and tend to follow the time course of the action potential (Fig. 5D). These monophasic current sources give rise to a monophasic extracellular potential with a magnitude that is largest at the site of the change in transmembrane potential and, based on the experimental data shown here (Figs. 2 and 3), occurs at the edge of the contact electrode.

Mechanism of Depolarization at the Contact Electrode site

It is not known why depolarization occurs in myocardial tissue exposed to the contact electrode. One explanation might be that pressure against the myocardium interrupts

local perfusion and thereby causes local ischemia with its known depolarizing effects on membrane potential. This mechanism is unlikely because MAP signals develop within seconds after stable contact with the myocardial surface is established¹; this is too rapid to cause significant metabolic alterations. A more plausible explanation is that the mechanical pressure of the MAP electrode against the myocardium produces shear stress and activates stretch-activated channels (SACs). The maximum depolarization measured nearest the contact electrode surface was around -23 mV (Fig. 3), which corresponds well with the equilibrium potential of SACs.¹⁶⁻¹⁸ Depolarization of tissue may depend on shear stress that is greatest at the electrode contact site. It can be assumed that shear stress still is high at the perimeter of the MAP electrode but falls off sharply just outside it, explaining the sharp border between membrane potential within and outside the perimeter of the contact electrode (Fig. 4).

Electrotonic Interaction

Even when V_m decreased below -50 mV (the value where excitability normally ceases), the microelectrode still recorded action potential waveforms. This may be due to electrotonic interaction, producing a passive “shadow” image of TAPs in nearby normal cells. It also indicates that electrical coupling remains. The sharpness of the border suggests that reported space constants of 0.5 to 1 mm for myocardial depolarization may not apply to the situation in this setting. The measurements here suggest a smaller length constant of about 100 to 200 μm . We hypothesize that shortening of the length constant is consistent with a reduced interstitial space under the contact electrode. Further studies are required to investigate the border sharpness as a function of the applied pressure to confirm this hypothesis.

Study Limitations

The actual shape of the cell volume depolarized by the contact electrode was not delineated in three dimensions but only two. We could only demonstrate that depolarization was greatest near the MAP electrode surface and, with increasing distance from the electrode center, gradually diminished toward near normal potentials at the epicardial surface. The difficult task of obtaining reliable TAP recordings prompted us to measure TAPs in only one plane, radiating from the MAP center. Nonetheless, there is no obvious reason to assume that the MAP electrode-induced depolarization is not similar in all directions. Another limitation was that we could not pinpoint the actual cell layer or micrometer distance from the contact electrode surface at which TAPs were recorded. This was due to two factors. First, contact electrode pressure against the RV wall distorted the natural geometry and compressed cell layers above it in a way that was hard to control by static measures. Second, due to the flexibility of the microelectrode tip and the compliance of the cardiac tissue, movement of the micromanipulator did not directly translate into movement of the microelectrode tip. We therefore used “layers” instead of actual calipered measurements of distance. Another limitation is that close to the contact electrode surface V_m was reduced and less useful as a guide to proper impalements, which may have resulted in inclusion of some data records with improper impalements rather than a truly de-

polarized membrane potential. This could bias our data toward more depolarized potentials and thus overestimation of the effect of the MAP electrode on membrane potential. Nonetheless, in 27 attempts we could never record a full action potential close to the MAP electrode surface, although the same microelectrode produced a full action potential immediately afterward at a distant site. Finally, the hearts were immobilized by BDM to facilitate stable microelectrode recordings. We recently showed that BDM altered the shape of the murine action potential but did so in both the MAP and TAP.⁵ These changes were a slowing of the upstroke (phase 0) and of repolarization phases 1 and 3. V_m was not significantly affected by BDM; therefore, it is unlikely that BDM interfered with the goal of this study.

Appendix

Current Sources Arising from Coupling Normal and Depolarized Cells

To explain the origin and shape of the time-varying transmembrane current near the MAP electrode, a simple three-cell circuit model (Fig. 5A) was developed. Summing currents at nodes 1–6 of Figure 5A yields:

$$I_i^1 = -I_m^1 \quad (1)$$

$$I_m^2 = I_i^1 - I_i^2 \quad (2)$$

$$I_i^2 = I_m^3 \quad (3)$$

$$I_e^1 = I_m^1 \quad (4)$$

$$I_m^2 = I_e^2 - I_e^1 \quad (5)$$

$$I_e^2 = -I_m^3 \quad (6)$$

and summing voltages around the two loops:

$$V_m^1(t) + I_e^1(t)R_e - V_m^2(t) - I_i^1(t)R_i = 0 \quad (7)$$

$$V_m^2(t) + I_e^2(t)R_e - V_m^3(t) - I_i^2(t)R_i = 0. \quad (8)$$

Substitution yields:

$$I_m^2(t) = \frac{V_m^1(t) - 2V_m^2(t) + V_m^3(t)}{R_i + R_e}. \quad (9)$$

Assuming a uniform propagation velocity of 65 cm/sec in the direction from left to right (cell 1 to cell 3) and a separation of 100 μm between cells, the intercellular propagation delay is $dt = 0.15$ msec. Assuming uniform velocity, the transmembrane potentials at the three nodes are the same function shifted in time, namely:

$$V_m^1(t) = V_m^2(t + dt) = V_m^3(t + 2dt). \quad (10)$$

As a result:

$$I_m^2(t) = \frac{V_m^1(t) - 2V_m^1(t + dt) + V_m^1(t + 2dt)}{R_i + R_e}. \quad (11)$$

To compute the current, a representative mouse transmembrane action potential (Fig. 5B) was used. If all cells have normal action potentials (Fig. 5B-I), then $I_m^2(t)$ has a biphasic time course reminiscent of a local electrogram, as shown in Figure 5C. Although the shape of $I_m^2(t)$ is not the same as

the extracellular potential, the work of Plonsey and Fleming¹³ shows that $I_m^2(t)$ is a good approximation near the surface of the tissue.

To simulate a MAP electrode placed over cell 3, a nonspecific linear leakage current I_l was added. I_l is expected to lower the membrane resistance in cell 3, where:

$$I_l(t) = g_l[V_m(t) - E_l]. \quad (12)$$

To a first approximation, the effect of this additional current can be given by:

$$\frac{dV_m}{dt} = -\frac{I_{ion}}{C_m} - \frac{I_l}{C_m} \quad (13)$$

so:

$$dV_m^l = \frac{dt I_l}{C_m} \quad (14)$$

$$V_m^3 = V_m^1 + dV_m^l \quad (15)$$

$$V_m^3 = V_m^1 + \frac{g_l(V_m^1 - E_l)dt}{C_m}. \quad (16)$$

When the leakage current with $g_l = 0.9 \text{ mS/cm}^2$, $E_l = -20 \text{ mV}$, $C_m = 1 \text{ mF/cm}^2$, and $dt = 15 \text{ } \mu\text{sec}$ is accounted for, the transmembrane potential under the MAP electrode is attenuated as shown in Figure 5B-II. As shown in Figure 5D, $I_m^2(t)$ is no longer biphasic but has a monophasic time course similar to the transmembrane action potential. In addition, roughly two thirds of the signal is below 0 mV as seen experimentally. This ratio is not expected to change because the scale factor $1/(R_i + R_e)$ is always positive.

References

1. Franz MR: Long-term recording of monophasic action potentials from human endocardium. *Am J Cardiol* 1983;51:1629-1634.
2. Hoffman BF, Cranefield PF, Lepeschkin E, Surawicz B, Herrlich HC: Comparison of cardiac monophasic action potentials recorded by intracellular and suction electrodes. *Am J Physiol* 1959;196:1297-1304
3. Schuetz E: Einphasische Aktionsstroeme vom in situ durchbluteten Saeugetierherzen. *Z Biol* 1932;92:78-90.
4. Franz MR, Burkhoff D, Spurgeon H, Weisfeldt ML, Lakatta EG: In vitro validation of a new cardiac catheter technique for recording monophasic action potentials. *Eur Heart J* 1986;7:34-41.
5. Knollmann BC, Katchman AN, Franz MR: Monophasic action potential recordings from intact mouse heart: Validation, regional heterogeneity, and relation to refractoriness. *J Cardiovasc Electrophysiol* 2001;12:1286-1294.
6. Ino T, Karagueuzian HS, Hong K, Meesmann M, Mandel WJ, Peter T: Relation of monophasic action potential recorded with contact electrode to underlying transmembrane action potential properties in isolated cardiac tissues: A systematic microelectrode validation study. *Cardiovasc Res* 1988;22:255-264.
7. Franz MR: Current status of monophasic action potential recording: Theories, measurements and interpretations. *Cardiovasc Res* 1999;41:25-40.
8. Schuetz E: Electrophysiologie des Herzens beim einphasischer Ableitung. *Ergebn Physiol Exp Pharmacol* 1936;38:493-620.
9. Franz MR: Method and theory of monophasic action potential recording. *Prog Cardiovasc Dis* 1991;33:347-368.
10. Yuan S, Blomstrom-Lundqvist C, Olsson SB: Monophasic action potentials: Concepts to practical applications. *J Cardiovasc Electrophysiol* 1994;5:287-308.
11. Scherrer-Crosbie M, Stuedel W, Hunziker PR, Foster GP, Garrido L, Liel-Cohen N, Zapol WM, Picard MH: Determination of right ventricular structure and function in normoxic and hypoxic mice: A transesophageal echocardiographic study. *Circulation* 1998;98:1015-1021.
12. Spach MS, Barr RC, Serwer GA, Kootsey JM, Johnson EA: Extracellular potentials related to intracellular action potentials in the dog Purkinje system. *Circ Res* 1972;30:505-519.
13. Plonsey R, Fleming DG: *Bioelectric Phenomena*. McGraw-Hill, New York, 1969.
14. de Mello WC, Motta GE, Chapeau M: A study on the healing-over of myocardial cells of toads. *Circ Res* 1969;24:475-487.
15. Sugarman H, Katz LN, Sanders A, Jochim K: Observations on the genesis of the electrical currents established by injury of the hearts. *Am J Physiol* 1940;130:130-143.
16. Craelius W, Chen V, El-Sherif N: Stretch activated ion channels in ventricular myocytes. *Biosci Rep* 1988;8:407-414.
17. Zabel M, Koller BS, Sachs F, Franz MR: Stretch-induced voltage changes in the isolated beating heart: Importance of the timing of stretch and implications for stretch-activated ion channels. *Cardiovasc Res* 1996;32:120-130.
18. Zeng T, Bett GC, Sachs F: Stretch-activated whole cell currents in adult rat cardiac myocytes. *Am J Physiol Heart Circ Physiol* 2000;278:H548-H557.